1.8A WILDFIRE EVOLUTION IN THE CONVECTIVE BOUNDARY LAYER

Ruiyu Sun[1] * Steven K. Krueger[1] Michael A. Zulauf[1] Mary Ann Jenkins[2] and Joseph J. Charney[3]
[1]University of Utah, Salt Lake City, Utah
[2]York University, Toronto, Canada
[3]United States Forest Service, North Central Research Station,East Lansing, MI

1. Introduction

Wildland fires mainly occur in the planetary boundary layer (PBL), even though their plumes can sometimes extend to levels above the PBL. Surface wind is one of the most important factors that affects how wildfires spread. Generally, the wind affects the fire's rate of spread (ROS) by tilting the fire flame, therefore changing efficiency of heat transfer to the unburned fuel and affecting the subsequent ignition of the fuel. There have been a number of experimental studies attempting to estimate the wildfire ROS based on the wind speed (Fons, 1946; Anderson and Rothermel, 1965; McArthur, 1966; Rothermel, 1972; Anderson et al., 1982; Forestry Canada Fire Danger Group, 1992; Cheney et al., 1993; Cheney et al., 1995, Cheney et al., 1998). A review up to 1990 on the wind effect on fires is given by Pitts (1991). Another review is given by Beer (1991) on the interaction of wind and fire. Recently, numerical models have also been used to study the relationship between the two. Morvan et al. (2002), using their physically based model, studied wind effects on the wildland fire propagation through Mediterranean shrub. Morvan et al. (2002) found that fire spread is dominately determined by the radiative and/or convective heat transfers depending on the wind conditions.

While the atmospheric flow is turbulent in nature in the atmospheric boundary layer (ABL) (Stull 1988) none of the previously listed studies has explicitly taken into account the effect of turbulence or gustiness of the winds on the growth of the wildland fires. Because of the interaction between the fires and the atmosphere, the average wind over a certain period does not necessarily have the same effect as the turbulent flow over the same period on the fire spread and intensity. Sudden changes in the wind often lead to erratic changes in the fire behavior and expose fire fighters to the extreme dangers (National Wildfire Coordinating Group, 1980). Being able to account for turbulence effect on the fire spread should improve the usefulness of ROS predictions, therefore increasing fire fighting safety and the efficiency of other fire suppression efforts, such as fire line breaks. For practical use, Crosby and Chandler (1966) created a table to help firefighters estimate gustiness based on the several hundred noon and afternoon observations made at Salem, Missouri, during fire seasons. Anderson et al. (1982) found a greater variation in the fire spread than in wind speed in grass fires in Australia.

Albini (1982a, 1982b) studied the response of free-burning fires to nonsteady wind by using a combination of an empirical representation of the power spectral density of near–surface gustiness in high winds and a theoretical model. He found that the variability of fire ROS was erratic with standard deviation exceeding the mean value for short periods of time in many fuels. In Albini's (1982a, 1982b) analyses, the interaction of the fire with the environment could not be included. This interaction could alter the ambient wind field significantly.

Taylor et al. (2004) analyzed the variation in the wind and crown fire behavior in northern jack pine–black spruce forest based on the fires during the International Crown Fire Modeling Experiment (ICFME) described by Stocks et al. (2004). Taylor et al. (2004) found that the ROS estimates during crown fires show considerable variation within distances of up to 150 m over periods of 1.5 – 10 min. They also found that the variance in ROS was greater than variance in wind speeds, and higher values were amplified.

In this study the University of Utah large eddy simulation–wildfire coupled model (UULES–wildfire coupled model) is used to take into account the fire induced flow due to the interaction between the fire and the atmosphere. The purpose is to examine how turbulence or gustiness in the ABL affects the spread of the fires and how the fires interact with the large eddies in the ABL. Two types of PBL are examined. One is a convective boundary layer (CBL) with noflow organization. The other one contains the convective rolls.

2. Numerical Experimental Set-up

The UULES–wildfire coupled model is used in this study. The UULES (Zulauf 2001) was specially de-

* *Corresponding author address:* Department of Meteorology, University of Utah, Salt Lake City, UT 84112. E-mail: rsun@met.utah.edu

signed to simulate small-scale atmospheric flows. It is coupled with a fire rate of spread formula (Hirsch 1996 or Rothermel 1972), a fuel consumption parameterization and a tracer code described by Clark et al. (2004). The coupling is implemented in such way that the energy from combustion is distributed into the atmosphere by using a extinction depth. The low level horizontal winds including the winds induced by the fires are fed into the fire spread formula. The coupled model has been evaluated against an Australian grass fire experiment F19 (Cheney et al. 1995) and a simulation of the grass fire experiment using wildland–urban interface fire dynamics simulator (WFDS, Mell et al. 2006), which includes a more physically based fire spread.

More than 20 simulations were completed. In all simulations, the domain size was 3200 m (x) $\times$ 3200 m (y) $\times$ 2000 m (z). The domain was covered by a grid mesh of 320 (x) $\times$ 320 (y) $\times$ 81 (z). The vertical grid was stretched and the minimum grid size was 5 m near the surface. A geostrophic wind of 5.5 m s^{-1} and constant with height was specified in each simulation.

To develop two different types of ABL, different surface heat fluxes and initial heights of the boundary layer top (z_i) were used. The values (from Moeng and Sullivan, 1994) are listed in the Table 1. In the CBL case, the surface heat flux was 240 W m^{-2} and initial z_i was 978 m. In the convective rolls case, they were 20 W m^{-2} and 468 m respectively. The convective velocities in the two types of ABL are also listed in the table.

The fuel was tall grass as in the Australian fire experiment. The empirical fire spread formula described by Hirsch (1996) was chosen. In the simulations, the winds at 5 m above ground level (AGL) were fed into the fire spread formula.

In order to efficiently examine the effects of boundary layer turbulence on the spread of fires, eight fires were ignited at the same time but in different locations in most of the simulations. In one case, just two fires were set. All fires in the simulations started after a steady state of the boundary layer statistics was reached. The fires lasted for 5 minutes in all simulations except for the two–fire case in which the fires lasted for 10 minutes.

3. Simulation Results

3.1. Fires in CBL

Figure 1 shows the vertical profiles of u, v and w variances (left) and the vertical profiles of the horizontal mean u, v and wind speed (right) in the CBL at 3600 s into the simulation. By this time the CBL has reached its steady state. The variances are in their forms similar to those described by Moeng and Sullivan (1994). The horizontal mean wind speed is approximately uniform through the boundary layer except near surface indicating a well-mixed boundary layer.

Table 1: Parameters for CBL and convective rolls

	CBL	convective rolls
Heat flux at surface (W m^{-2})	240	20
initial z_i (m)	937	468
convective velocity (w_*,m s^{-1})	2.0	0.7

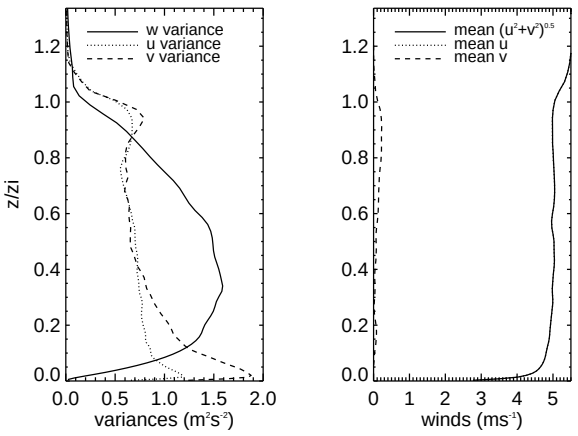

Figure 1: Vertical profiles of w, u, and v variances (left) and horizontal means of u, v and horizontal wind speed (right) in the CBL at the 3600 sec into the simulation.

At this time, 8 same fires were ignited at different locations. The initial fire line length (L_{ig}) was 200 m. The 8 fires evolved differently. Figure 2 shows the fire lines of 8 fires at the end of the 5–minute simulation. Not only the shapes of the fire lines are quite different among the 8 fires, but also the burnt areas. The largest area burnt is about twice as big as the smallest one. Associated with each fire, during its evolution, were variations in the rate of spread (ROS) and direction of spread due to the changes in the wind speed and direction at the fire line.

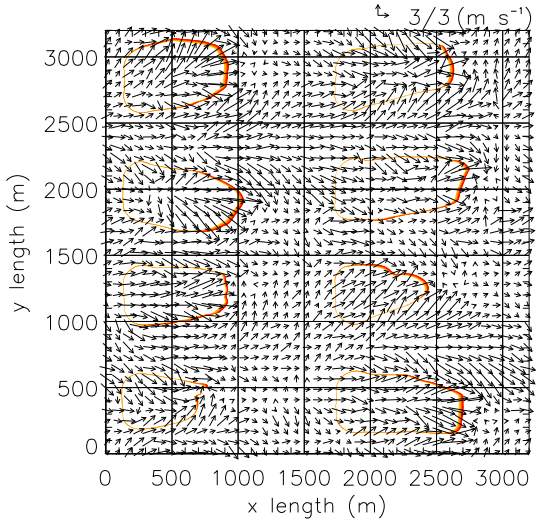

Figure 2: Fire lines of 8 fires (initial fire line length was 200 m) in the CBL at 5 mins after the fires started. Arrows are the horizontal wind vectors at 5 m AGL.

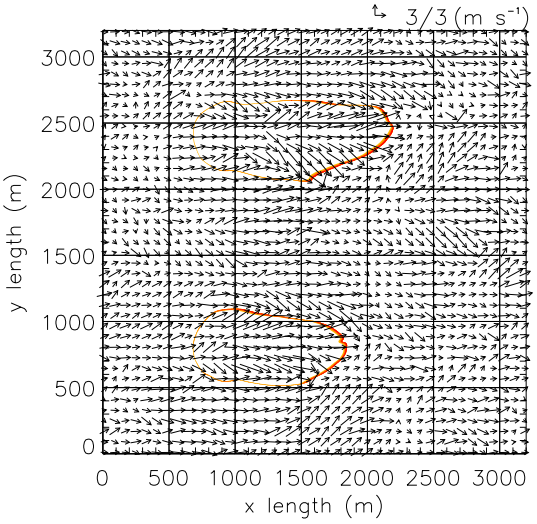

Figure 3: Fire lines of 2 fires (20 m L_{ig}) in the CBL at 10 minutes after the fires started. Arrows are the horizontal wind vectors at 5 m AGL.

Wildland fires usually do not start large but grow large from small fires that are in favorable conditions. To examine how small fires grow large two small fires were ignited with 20 m L_{ig}. Figure 3 shows the fire lines of the two fires at the end of the 10–minute simulation. One of the fires burnt an area considerably larger than the other one. The reason for the difference in the burnt area is evident in Figure 4, which shows the time histories of the maximum ROS associated with the two individual fires. In the first 100 seconds, the difference in the maximum ROS was small between the two fires. But the maximum ROS associated with one fire (blue) doubled in the time from 100 s to 200 s while the maximum ROS for the other fire (black) stayed about the same. The resulting difference in the maximum ROS between the two fires remained almost constant for the rest of the simulation and lead to the difference in the burnt area between the two fires.

Why are there such big differences among the 8 fires shown in Figure 2 and the 2 fires in Figure 3? Given that a homogeneous fuel bed and flat terrain were used in the simulations, the only factor that could make the same initial fires evolve differently is the wind (speed and direction) at 5 m AGL. The wind was a combination of the ambient wind and the fire–induced wind. In the CBL, the ambient wind was turbulent. It will therefore contribute to the differences among the fires.

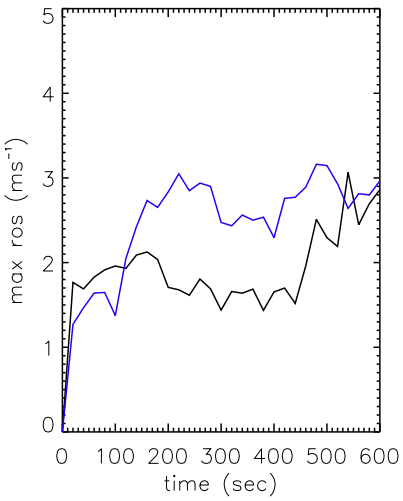

Figure 4: Time histories of maximum ROS associated with the two fires (20 m L_{ig}) in the CBL.

Fires can also generate circulations due to their buoyant plumes. In addition, the fire plumes might interact with the large eddies in the CBL to produce differences in the wind. So both the ambient wind and the fire induced wind produced the differences among the fires. Which one is the main contributor, the am-

bient turbulent wind or the fire induced wind ? To address this question, the wind has to be separated into the two components. The separation was implemented by turning off the addition of the energy from the fires into the UULES atmosphere. This means that no flow was induced by the fires and the fires were only driven by the ambient wind. We named this type of coupling 'one–way coupling', and the previous coupling method 'two-way coupling'. The 'one–way coupling' model behaves like an operational firespread prediction model, such as FARSITE (Finney 1998). The same simulation such as shown in Figure 2 was re-computed using the 'one–way coupling' method.

Figure 5 shows the overlay of the fire lines of 8 fires for the 'two-way coupling' case (yellow) and the fire lines of 8 fires for the 'one–way coupling' case (blue) at the end of the 5–minute simulations. Fires in the 'one–way coupling' case burnt smaller areas than those in the 'two-way coupling' case. There were variations in the fire line shape and the burnt area among the 8 fires in the 'one–way coupling' case. But the variations were much smaller than those in the 'two-way coupling' case, indicting that the fire–induced flow was mainly responsible for the differences among the 8 fires in the Figure 2. The fires in the 'one–way coupling' case tended to spread to the flanks of the fires a little more than that in the 'two–way coupling' case. This suggests that the fire induced wind mainly spread the fires in the downwind direction.

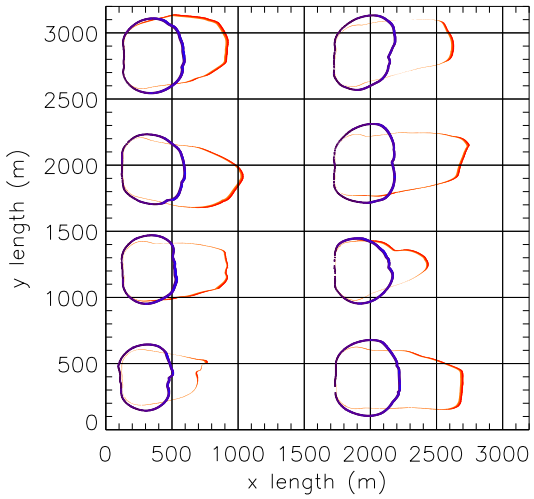

Figure 5: Overlay of fire lines of 8 fires (200 m L_{ig}) in the 'two–way coupling' case (yellow) and 'one–way coupling' (blue) case in the CBL at 5 mins after the fires started

To quantify the differences among the fires in the CBL, the frequency distributions of several fire variables were calculated based on 24 fires from 3 8–fire simulations. The time interval between the 3 simulations was 5 minutes, longer than the integral time scale of the turbulent motion. Figure 6 shows the time histories of the cumulative frequency distributions of burnt areas of 24 fires in the 'two–way' coupling case (left) and in the 'one–way coupling' case (right). In each plot the black (blue) line represents the smallest (largest) area burnt among the 24 fires. The red line represents the median area. Both the sizes of the burnt areas and the differences among the 24 fires in the 'one–way coupling' case are about half of those in the 'two–way coupling' case. The largest burnt area in the 'one–way' coupling case is about the same as the smallest one in the 'two–way coupling' case. In the 'two–way coupling' case, the largest burnt area is more than twice as big as the smallest. These results indicate that the fire–induced wind was the main contributor to the differences among the fires in the CBL.

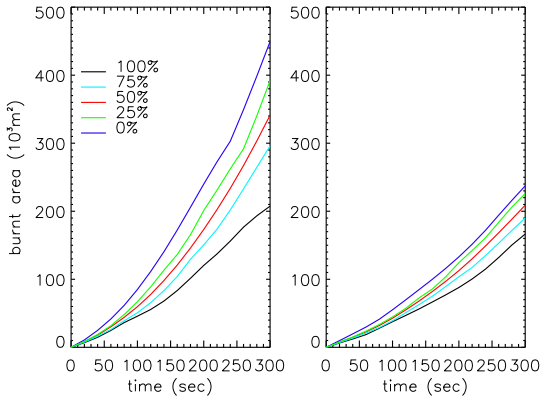

Figure 6: Time histories of the cumulative frequency distributions of the burnt areas based on 24 fires in the 'two-way coupling' case (left) and 'one-way coupling' case (right) in the CBL

Figure 7 illustrates the time histories of cumulative frequency distributions of maximum ROS in the 'two-way coupling' case and in the 'one-way coupling' case. Both the maximum ROS and the differences among them in the 'two-way coupling' case are significantly larger than that in the 'one–way coupling' case.

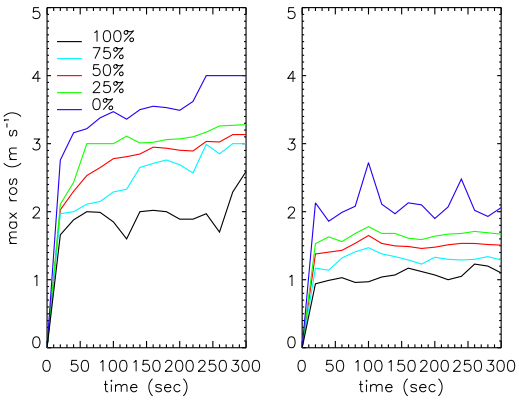

Figure 7: Time histories of the cumulative frequency distributions of the maximum ROSes based on 24 fires in the 'two-way coupling' case (left) and one-way coupled case (right) in the CBL

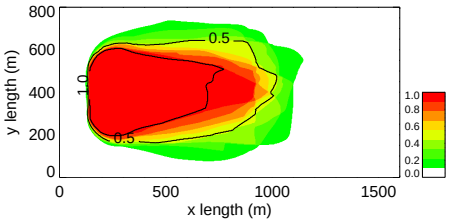

Figure 8: Burn probability based on 24 fires (200m L_{ig}) in the CBL at 5 mins after the fires started.

To further illustrate the differences among the fires in the CBL, burn probabilities were calculated based on 24 fires in both 'two-way coupling' case and 'one-way coupling' case at the end of the 5-minute simulations. These are shown in Figures 8 and 9. In each figure, the contours labeled 1.0 indicates that the region inside the contour was burnt by all 24 fires. The 0.5 contour indicates that the region inside the contour was burnt by at least 12 fires. The outermost shaded contour shows the area burnt by at least one fire. In the 'two–way coupling' case the fires spread over a large area. In the 'one-way coupling' case, all the fires were contained in a smaller area, but there was still uncertainty about burning between the 1.0 contour and outermost shaded contour. This uncertainty might be bigger than the uncertainty in the ROS formula due to its empirical nature. Since the 'one–way coupling' model behaves like operational models, Figure 9 suggests that fire spread is not deterministic in the CBL even if the fire–induced wind is not considered. The turbulent flow in the CBL affects how a fire spreads. A probabilistic prediction of the fire spread that can take into account the random components might make the fire spread formula currently used in the operational model more useful. In the 'two–way coupling' case the uncertainty is much bigger than the 'one–way coupling' case. This again suggests the potential importance of the probabilistic prediction of the fire spread.

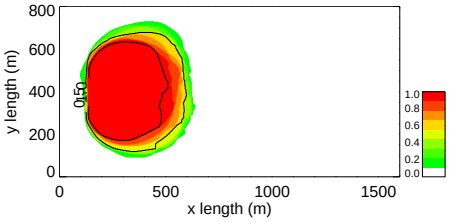

Figure 9: Burn probability based on 24 fires (200m L_{ig}) from the one-way coupled case in the CBL at 5 mins after the fires started.

3.2. Fires in convective rolls

Figure 10 shows the profiles of the u, v and w variances (left plot) and the profiles of the horizontal mean u, v and wind speed (right plot) in the ABL with convective rolls at 5400 s into the simulation. A steady state ABL has been achieved by this time. Compared with the properties in the CBL, variances are smaller due to the smaller surface heat flux and depth of the boundary layer. The wind speed was also smaller at 5 m AGL in the convective rolls.

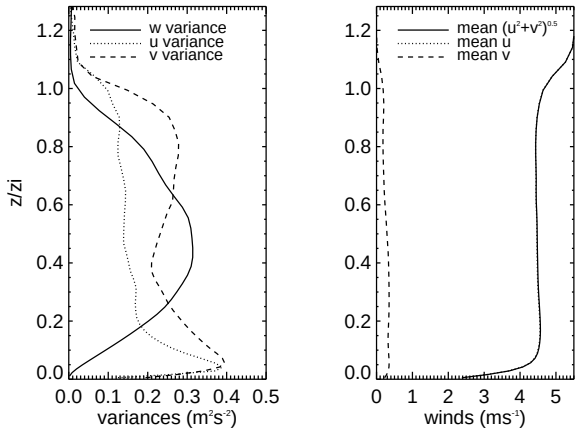

Figure 10: Vertical profiles of w, u, and v variances (left) and horizontal means of u, v and horizontal wind speed (right) in the ABL with the convective rolls at the 5400 sec into the simulation.

Figure 11 shows the vertical velocity at 147 m AGL, about 1/3 of the ABL depth, and the horizontal winds at 5 m AGL. The convective rolls were are obvious. There were variations in the surface wind speed and direction, but not as large as in the CBL case. Weak convergence of winds at 5 m AGL occurred underneath the updraft region of the convective rolls and weak divergence underneath the downdraft region of the convective rolls. The purpose of studying fires in this type of boundary layer is to examine how the variations in the winds and their convergence and divergence affect the spread of the fires and how differently the fires evolve.

8 fires were ignited in the convective rolls. The fires had the same L_{ig} and were ignited at the same locations as the 8 fires in the CBL. Figure 12 shows the fire lines of 8 fires at the end of a 5-minute simulation. There are differences in the fire line shape and burnt area among the fires. But the differences are not as significant as that among the fires in the CBL shown in Figure 2. One reason for this is that the turbulence was not as intense in the convective rolls case as in the CBL case. Because the convergence and divergence were weak compared to the fire–induced winds it is hard to see the effects of the divergence and convergence on the evolution of the fires. Only the top two fires in Figure 12 were mainly located in a convergence region during the simulation. All other fires were in divergence regions. The areas burnt by the two fires in the convergence regions are relatively small compared with the other fires. To see this effect more clearly, stronger convergence and divergence have to be developed at the level where fires spread.

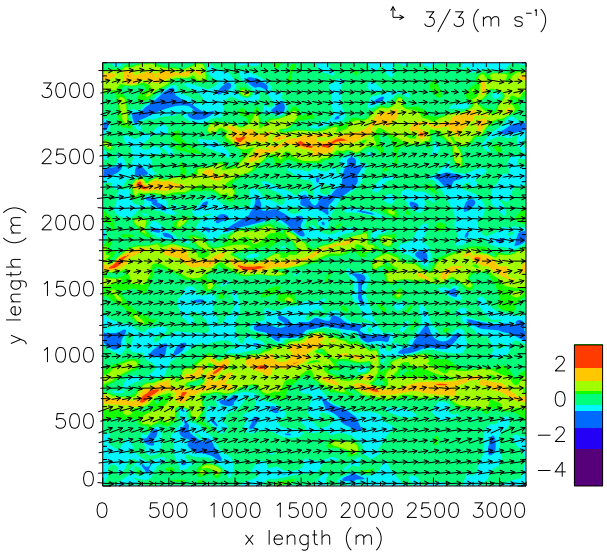

Figure 11: Vertical velocity at 147 m AGL in the ABL with the convective rolls at 5400 sec into the simulation. Arrows are horizontal wind vectors at 5 m AGL.

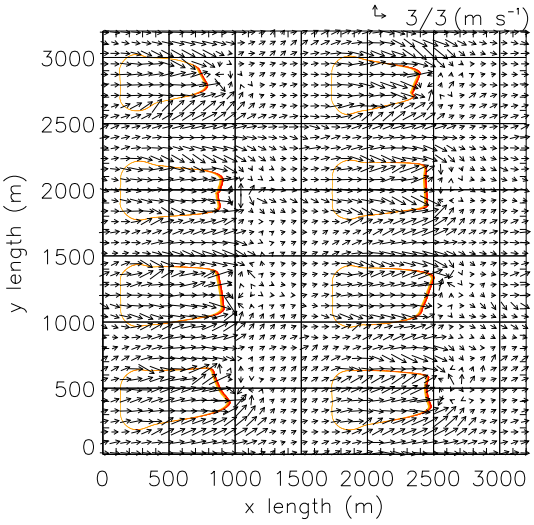

Figure 12: Fire lines of 8 fires (200 m L_{ig}) in the ABL with convective rolls at 5 mins after the fires started. Arrows are the horizontal wind vectors at 5 m AGL.

Time histories of the cumulative frequency distributions of the burnt area and the maximum ROS are calculated based on 24 fires in the convective rolls and are shown in the Figure 13. Compared with the corresponding plots in the CBL case in the Figure 6 and

Figure 7, the minimum values of the burnt area and the maximum ROS are about the same in the convective rolls as in the CBL. But variations in both variables are smaller in the convective rolls than in the CBL. This is also shown in the Figure 14. Figure 14 presents the burn probabilities based on 24 fires. Due to less intense turbulence, fires in the convective rolls tend to burn towards the flanks of the fires less than in the CBL. The difference between the 1.0 contour and the outmost shaded contour in Figure 14 is not as big as in the Figure 8.

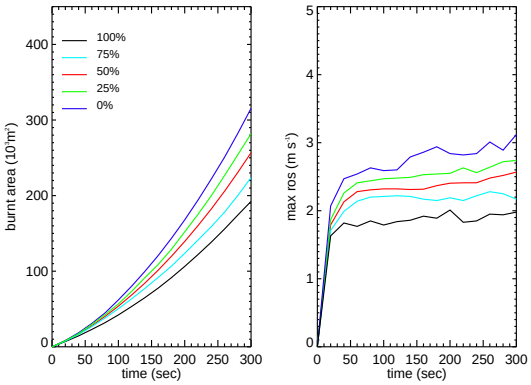

Figure 13: Time histories of the cumulative frequency distributions of the burnt area and maximum ROS based on 24 fires in the CBL.

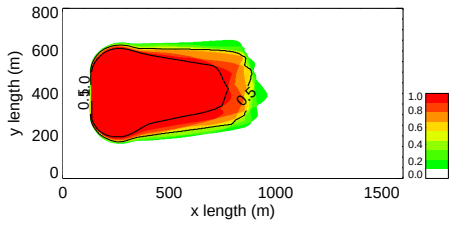

Figure 14: Burn probability based on 24 fires (initial fire line length was 200m) in the ABL with convective rolls at 5 mins after the fires started.

3.3. Effect of L_{ig} on the fire variation

In the CBL, turbulence may have different effects on different sizes of fires. To investigate this, 6 different L_{ig}s were used to simulate fires in CBL. The L_{ig}s were 20 m, 50 m, 100 m, 150 m, 200 m, and 250 m. For each L_{ig}, 3 simulations with 8 fires in each (totally 24 fires) were completed. The left plot in the Figure 15 shows the mean burnt area of 24 fires and the standard deviation of burnt areas of 24 fires for each L_{ig}. The standard deviation generally increases as L_{ig} decreases. The maximum difference among the standard deviations is about 25% of the minimum standard deviation. There are hardly any differences between the standard deviations of the 20 m and 50 m L_{ig}s and between the standard deviations of the 200 m and 250 m L_{ig}s. The growth of the standard deviations are mainly due to the growth of the mean burnt areas. In the right plot, the vertical axis is the standard deviation normalized by the corresponding mean burnt areas. It shows that the normalized standard deviation approximately ranges from 0.17 to 0.25 after the fires reach larger sizes. The standard deviations in the convective rolls ABL for the 200 m L_{ig} case are also shown in the two plots. Standard deviations are smaller in the convective rolls than in the CBL. Figure 15 suggests that it

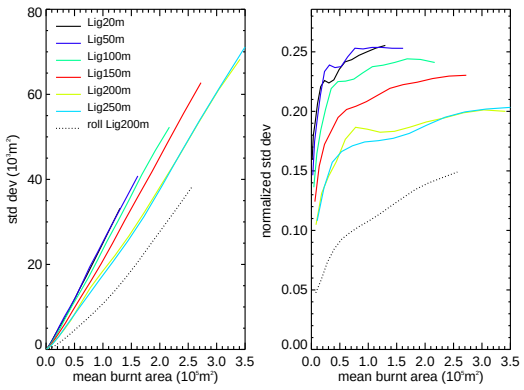

Figure 15: Mean burnt area versus standard deviation (left) of burnt areas of 24 fires and mean burnt area versus standard deviation normalized by the mean burnt area (right) of 24 fires for each initial fire line length case in the CBL and ABL with the convective rolls.

might be possible to parameterize the variability of burnt area. Such a parameterization would allow operational models which do not account for effects of turbulence on fires to predict how fires spread in a more realistic way.

3.4. Mechanisms of fire–induced flow and its effect on fire spread

As shown in section 3.1, the differences among the fires in the CBL were mainly due to the fire–induced wind. How was the fire–induced wind generated? How did the fire–induced wind affect the fire spread? We believe that there are two main mechanisms for producing fire–induced flows in the CBL. The first one was suggested by Clark et al. (1996). Clark et al. argued that, in a mean ambient wind, the convective column is tied to the fire at the surface and tilts downstream with height. The effect of downstream tilting is to shift the center of the low-level convergence pattern ahead of the fire front. If this convergence zone remains in front of but adjacent to the fireline, then a flow will be continuously induced across the fire line. The other mechanism for the fire–induced flow is the downdraft behind the fire line. It is generated by the interaction between the fire plume and the large eddies in the CBL.

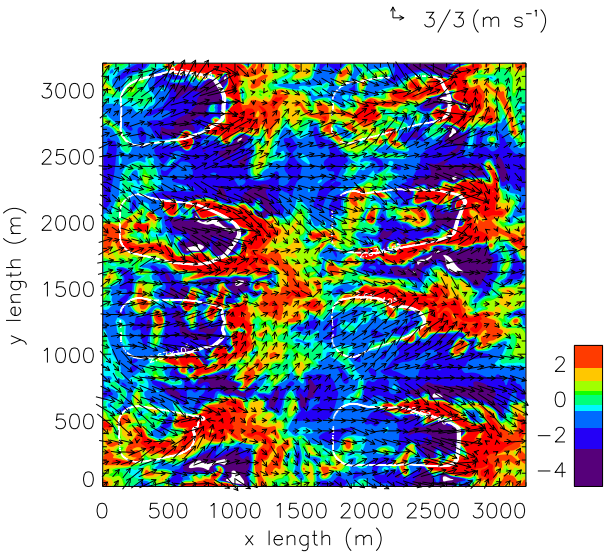

Figure 16: Vertical velocity at 147 m AGL (colored contour). Fire lines are white. Arrows are wind vectors at 5 m AGL.

Figure 16 shows the vertical velocity at 147 m AGL and the horizontal wind vectors at 5 m AGL at the end of a 5–minute fire simulation in the CBL. The white contours are the fire lines. Ahead of each fire there is a convergence zone, that induces a flow across the head fire line. Behind the head fire lines of most large fires there are strong downdrafts. An exception is the fire at the top right. Behind the head fire lines of the two small fires (left bottom fire and second fire from the bottom on the right), there is either an updraft or a weak downdraft.

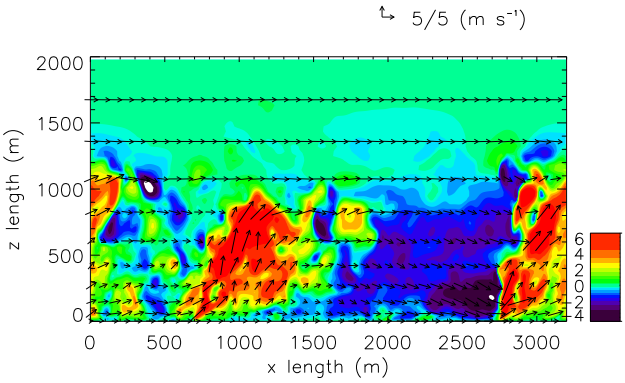

Figure 17: X–Z vertical cross-section of vertical velocity through y = 400 m.

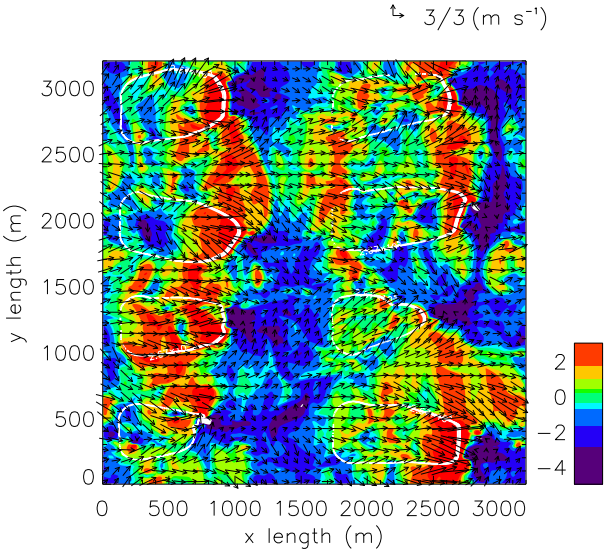

Figure 18: Like Figure 16 for u perturbation at 5 m AGL.

The role of the downdrafts behind the fire lines is to bring down higher momentum air from aloft to the height level at which fires spread. Figure 17 shows a vertical cross section of the vertical velocity field along y = 400 m in Figure 16 through a large fire and a small fire at the end of 5–minute simulation. The small fire is mainly in the updraft region. It stayed in the up-

draft region throughout most of the simulation. Even through in the early stage of the simulation the small fire had a downdraft behind it, the downdraft did not remain behind the fire. Behind the large fire there was a strong downdraft. The large fire started in the downdraft region. The fire plume enhanced the downdraft behind it and the downdraft remained behind the fire throughout the simulation. This downdraft continuously transported higher momentum air from upper to low levels. The increased wind spread made the fire burn an larger area than the fire in the updraft region.

Figure 18 shows the perturbation field of u (wind in west–east direction) at 5 m AGL at the end of the simulation. Large fires are associated with the positive perturbations behind the head fire lines. The perturbations associated with small fires are apparently weaker. This pattern remained in place for most of simulation time, and explained why the large fires grew large and the small fires had smaller burnt areas.

4. Conclusions

This study has examined the evolution of grass fires in two types of the ABL, the CBL and convective rolls. Fires grow differently under the same boundary layer conditions. The development of the fires has a significant random component. Fire spread is not deterministic in the ABL. A probabilistic prediction method is warranted. In the CBL, the fire induced flow appears to be the main contributor to the variability of the fires. One of the mechanisms for the induced flow is the downdraft behind the head fire line. It is the result of the interaction between the fire induced circulation (fire plume) and the large eddies in the ABL. If the downdraft remains behind the head fire line, the fire is in a favorable configuration to grow larger. The effect of the initial fire line length on the variations among the fires in the CBL is also examined. The variation among the fires increases as the initial fire line length decreases. But this effect is not strong. The variation among the fires increases mainly due to the growth of the fires. Fires in the convective rolls ABL are less variable than in the CBL in this study. One reason is that the turbulent motion in the convective rolls ABL was less intense.

References

Albini, F., 1982a: Response of free burning fires to nonsteady wind. *Combust. Sci. and Technol.*, **29**, 225–241.

Albini, F., 1982b: The variability of wind–aided free burning fires. *Combust. Sci. and Technol.*, **31**, 303–311.

Anderson, H., E. Catchpole, J. MeMestre, and T. Parkes, 1982: Modeling the spread of grass fires. *J. Aust. Math. Soc.*, **23**, 312–319.

Anderson, H., and R. Rothermel, 1965: Influence of moisture and wind upon the characteristics of free–burning fires. *Tenth Symposium (International) Combustion. Proc.*, Combust. Inst., 1009–1019.

Beer, T., 1991: The interaction of wind and fire. *Boundary Layer Meteorology*, **54**, 187–308.

Cheney, N., and J. Gould, 1995: Fire growth in grassland fuels. *International J. of Wildland Fire*, **5(4)**, 237–247.

Cheney, N., J. Gould, and W. Catchpole, 1993: The influence of fuel, weather and fire shape variables on fire–spread in grasslands. *International J. of Wildland Fire*, **3(1)**, 31–44.

Cheney, N., J. Gould, and W. Catchpole, 1998: Prediction of fire spread in grassland. *International J. of Wildland Fire*, **8(1)**, 1–13.

Clark, T., J. Coen, and D. Latham, 2004: Description of a coupled atmosphere-fire model. *International J. of Wildland Fire*, **13**, 49–63.

Clark, T., M. A. Jenkins, J. Coen, and D. Packham, 1996: A coupled atmosphere-fire model: role of the convective froude number and dynamic fingering at the fireline. *International J. of Wildland Fire*, **6**, 177–190.

Crosby, J., and C. Chandler, 1966: Get the most from your windspeed observation. *Fire Control Notes*, **27**, 12–13.

Finney, M. A., 1998: FARSITE: Fire Area Simualtor-Model, Development and Evaluation. Technical Report RMRS-RP-4, USDA Forest Service, Rocky Mountain Research Station Paper.

Fon, W., 1946: Analysis of fire spread in light forest fuels. *J. Agric. Res.*, **72(3)**, 93–121.

Forestry Canada Fire Danger Group, 1992: Development and structure of the Canadian forest fire behavior prediction system. Technical Report Inf Rep. ST-X-3, Can. For. Serv.

Hirsch, K. H., 1996: Canadian forest fire behavior prediction (fbp) system: User's guide, special report 7. Technical report, Canadian Forest Service, Northwest Region, Northern Forestry Center.

McArthur, A., 1966: Weather and grass fire behavior. Department of National Development, Forestry and Timber Bureau, Canberra, Leaflet 100,23pp.

Mell, W., M. A. Jenkins, J. Gould, and P. Cheney, 2006: A physically based approach to modeling grassland fires. *International J. of Wildland Fire*, **under review**.

Moeng, C.-H., and P. Sullivan, 1994: A comparison of shear and buoyancy driven planetary-boundary-layer flows. *J. Atmos. Sci.*, **51**, 999–1022.

Morvan, D., V. Tauleigne, and J. Dupuy, 2002: Wind effects on wildfire propagation through a mediterranean shrub. *Forest Fire Research and Wildland Fire Safety*, Millpress, Rotterdam. ISBN 90-77017-72-0.

Pitts, W., 1991: Wind effects on fires. *Prog. Energy Combust. Sci.*, **17**, 83–134.

Porterie, B., D. Morvan, J. Loraud, and M. Larini, 2000: Firespread through fuel beds: Modeling of wind-aided fires and induced hydrodynamics. *Phys. Fluids*, **12**(7), 1762–1782.

Rothermel, R., 1972: A mathematical model for predicting fire spread in wildland fuels. *Research paper INT 115, Intermountain Forest and Range Experiment Station Ogden, Utah, USA*.

Stocks, B., M. Alexander, B. Wotton, C. Stefner, M. Flannigan, S. Taylor, and et al., 2004: Crown fire behavior in a northern jack pine–black spruce forest. *Can. J. For. Res.*, **34**, 1548–1560.

Stull, R. B., 1988: *An Introduction to Boundary Layer Meteorology*. Kluwer Academic Publishers.

Taylor, S., B. Wotton, M. Alexander, and G. Dalrymple, 2004: Variation in wind and crown fire behavior in a northern jack pine–black spruce forest. *Can. J. For. Res.*, **34**, 1561–1576.

Zulauf, M.A., 2001: *Modeling the effects of boundary layer circulations generated by cumulus convection and leads on large–scale surface fluxes*. PhD thesis, University of Utah.

ACKNOWLEDGMENTS. This research was supported by the United States Department of Agriculture Forest Service Research Joint Venture Agreement 03-JV-11231300-08. A gratis grant of computer time from the Center for High Performance Computing, University of Utah, is gratefully acknowledged.